A thermal energy storage process for large scale electric applications

T Desrues, J Ruer, P Marty, Jf Fourmigué

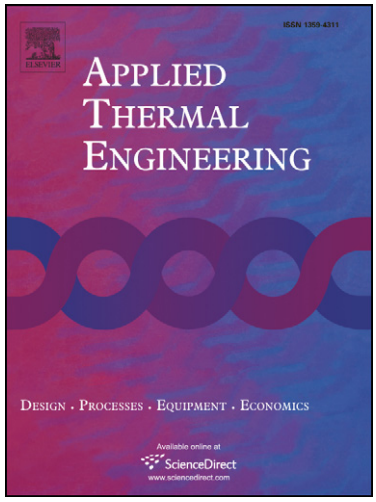

A thermal energy storage process for large scale electric applications

T Desrues, J Ruer, P Marty, JF Fourmigué

PII: S1359-4311(09)00293-2
DOI: 10.1016/j.applthermaleng.2009.10.002
Reference: ATE 2898

To appear in: *Applied Thermal Engineering*

Received Date: 20 May 2009
Accepted Date: 1 October 2009

Please cite this article as: T. Desrues, J. Ruer, P. Marty, J. Fourmigué, A thermal energy storage process for large scale electric applications, *Applied Thermal Engineering* (2009), doi: 10.1016/j.applthermaleng.2009.10.002

A thermal energy storage process for large scale electric applications

T Desrues[*1,2], J Ruer[1], P Marty[3], JF Fourmigué[2]

[1] SAIPEM-SA, 1/7 avenue San Fernando, 78884 Saint-Quentin en Yvelines, France
[2] CEA, DRT/LITEN/DTS/LETh-GREThe, 17 rue des Martyrs, 38054 Grenoble, France
[3] LEGI, BP 53, 38041 Grenoble Cedex 9, France

Abstract: A new type of thermal energy storage process for large scale electric applications is presented, based on a high temperature heat pump cycle which transforms electrical energy into thermal energy and stores it inside two large regenerators, followed by a thermal engine cycle which transforms the stored thermal energy back into electrical energy. The storage principle is described, and its thermodynamic cycle is analyzed, leading to the theoretical efficiency of the storage system. A numerical model is developed, and the results show the feasibility of the process, even with sub-optimal parameters. Finally, key factors for improving the process performances are identified.

Keywords: Energy storage, Turbomachine, Regenerator, Heat transfer, Brayton cycle, Numerical model.

[*] Corresponding author. Tel.: +33 438780603
E-mail address: tristan.desrues@cea.fr

Nomenclature

Bi	Biot number	[.]
c_p	Specific heat at constant pressure	[J/K/kg]
c_v	Specific heat at constant volume	[J/K/kg]
d_h	Hydraulic diameter	[m]
e	Specific energy	[J/kg]
H	Height	[m]
h	Convective heat exchange coefficient	[W/m²/K]
L	Length	[m]
$\dot{m}$	Mass flow rate	[kg/s]
N_{ch}	Number of channels	[.]
Nu	Nusselt number	[.]
$\mathcal{P}$	Power density	[W/m^3]
PR	Pressure Ratio	[.]
S	Section, Surface	[m^2]
t	Time	[s]
T	Temperature	[K]
Tol	Temperature relative tolerance	[.]
v	velocity	[m/s]
W	Width	[m]
z	Axial coordinate	[m]

Greek letters

α	Void fraction	[.]
ε	Energy storage efficiency	[.]
δ	Thickness	[m]
γ	c_p/c_v	[.]
λ	Thermal conductivity	[W/m/K]
ψ	Thermal compression ratio	[.]
η	Polytropic efficiency	[.]
ρ	Density	[kg/m^3]

Subscripts

0	Environment point
1	High temperature point, loading period
2	Mid temperature point, delivery period
3	Low temperature point
comp	Compressor
ch	Channel
charac1	Turbomachine characteristic linking PR and $\dot{m}_r$
charac2	Turbomachine characteristic linking η and $\dot{m}_r$ or PR
deliv	Delivery period
exch	Exchange
f	Fluid
HP	High Pressure
is	Isentropic
load	Loading period
LP	Low Pressure

max	Maximum
nom	Nominal value
r	Reduced
s	Solid
th	Theoretical
tot	Total
turb	Turbine

1. Introduction

Electric energy storage is currently gaining interests from the governments of the USA, the EU, Japan and Australia, for numerous reasons including the deregulation of the electricity market, the growth of renewable energies [1], and the need for network flexibility in terms of load leveling [2]. There are currently several more or less mature storage technologies, each one having its own scale of application. Currently, it exists three large scale applications, typically greater than 10 MWh: Pumped Hydroelectric Storage (PHS) consists in elevating water in an upper reservoir, what allows storing up to several GWh. Compressed Air Energy Storage (CAES) systems use a cavern to store pressurized air and offers a capacity of several hundreds of MWh. Flow batteries, in which the electrolyte contains dissolved electroactive species flowing through a power cell/reactor, can store several hundreds of MWh too, but provide a more limited output power.

Thermal energy storage already exists in a wide spectrum of applications. Sensible heat storage is used in pebble bed, packed bed or molten salts for thermal solar power plants [3], in water heater storage [4], in blast or glass furnace regenerators [5], and it is the most used technology for heating and cooling of buildings [3]. Latent heat storage is used in buildings for passive storage systems such as phase change material walls, wallboards, and shutters [3], in solar latent heat storage unit [6,7], or for the cooling of transient thermal load of electronic devices [8].

However, as far as we know, thermal energy storage has not been developed for electric storage yet, and this paper presents a new thermal energy storage process for large scale electric applications, that does not suffer from geographical constrains such as the need for a large altitude difference between two large water reservoirs for Pumped Hydroelectric Storage, or large cavern for Compressed Air Energy Storage [9,10].

2. Storage principle

The system consists of a HP (High Pressure) tank and a LP (Low Pressure) tank, four turbomachines (one compressor/turbine pair used during the loading period, and another one during the delivery period), and two heat exchangers (Figure 1). The tanks are regenerators, made of refractory material which will alternatively store or deliver heat. The turbomachines allow the circulation of a gas (Argon) in the tanks, following a closed thermodynamic Brayton cycle. In Figure 1, the gas flows clock-wise during the loading period and counter clock-wise during the delivery period. For clarity, only one of the two pairs of turbomachines is shown.

2.1. Loading period

Let us assume that the initial temperature of the HP tank is $T_0 = T_{0nom,}$ which is equal to the outside temperature (≈ 25 °C), while the initial temperature of the LP tank is $T_2 = T_{2nom} \approx 500$ °C (Figure 2). The turbomachines force the gas to follow the route 0,3,2,1, which corresponds to a heat pump cycle, taking heat from the LP tank to bring it to the HP tank. The temperature at the compressor outlet (cycle point 1) is $T_1 \approx 1000$°C, and the temperature at the turbine outlet (cycle point 3) is $T_3 \approx -70$°C. The HP tank refractory material initially at T_0 is slowly heated by the hot gas entering at T_1, while the LP tank material initially at T_2 is slowly cooled by the cold gas entering at T_3. This generates two transient thermal fronts, progressing upward in the LP tank and downward in the HP tank.

When the thermal fronts will approach the ends of the tanks, the HP tank temperature T_0 will suddenly increase while the LP tank temperature T_2 will decrease. Hot and cold heat exchangers are necessary to keep the inlet turbomachine temperatures at their nominal values. The loading is stopped when the temperature differences between one tank's outlet and its prescribed nominal temperature exceeds a given relative threshold, named *Tol*.

2.2. Delivery period

During the delivery period (Figure 3), the gas follows the route 1,2,3,4,0 which corresponds to a heat engine cycle. Let $T_4 \approx 60$ °C be the compressor outlet temperature, while $T_0 \approx 25$ °C is the cold exchanger outlet temperature, and $T_2 \approx 500$°C is the temperature after expansion at the turbine outlet. Similarly to the loading period, the LP tank refractory material at T_3 is slowly heated by warm gas at T_2, while the LP tank material at T_1 is slowly cooled by gas at ambient temperature T_0, again generating two transient thermal fronts.

Turbomachine irreversibilities being taken into account, a part of the incoming and outgoing work is transformed into additional heat. This results in an irreversible heat production, which must be evacuated from the system, and this is done through the cold exchanger, shown at the bottom of Figure 3.

Similarly to the loading period, the delivery period is stopped when the relative temperature differences between one tank outlet and its prescribed nominal temperature exceeds the threshold *Tol*.

2.3. Capacity and efficiency

Let us use the subscripts 1 for loading, and 2 for delivery. The capacity is defined as the delivered energy $E_{network2}$ (Figure 4), and the efficiency is defined as the ratio of $E_{network2}$ to $E_{network1}$.

Figure 4 shows energy flows exchanged with outside, during loading and delivery periods. The transformation between electric energy and mechanical energy is considered having 100% efficiency, as well as the transformation between electric energy and thermal energy inside the hot exchanger. The arrows width is representative of the flows magnitude.

Actually, the system needs a certain number of transient loading and delivery cycles before reaching a steady periodic state. This is because the two thermal fronts tend to slowly enlarge, and the steady periodic state is only reached when this enlargement is exactly compensated by the temperature correction performed by the cold and the hot heat

exchangers when the fronts arrive at the ends of the tanks. During the first cycles, capacity and efficiency may show significant variations.

3. Thermodynamic analysis

This section aims at discussing the theoretical global storage efficiency as a function of the turbomachines polytropic efficiency η, the pressure ratio PR, the c_p to c_v ratio γ, and the initial temperatures T_{0nom} and T_{2nom}, neglecting head losses in the flow, and assuming the system is adiabatic. Since the thermal insulation losses are related to the heat transfer area to volume ratio, the larger the regenerators, the more accurate the adiabatic assumption is.

3.1. Polytropic process

The gas is considered as ideal. To take account of the turbomachine irreversibilities, polytropic process is convenient since the polytropic efficiency doesn't depend on the compression ratio [11].

Using the *thermal compression ratio* notation [12] :

$$\psi = (PR)^{\frac{\gamma-1}{\gamma}} \tag{1}$$

where PR is the pressure ratio, and using the polytropic efficiency η, one can write, for a compression:

$$T_{outlet} = T_{inlet} \times \psi^{1/\eta} \tag{2}$$

and for an expansion:

$$T_{outlet} = T_{inlet} \times \psi^{-\eta} \tag{3}$$

If η = 1, equations (2) and (3) reduce to the usual equation for the adiabatic and isentropic compression of an ideal gas. Because η is lower than 1 for an irreversible process, the outlet machine temperature is always greater in the irreversible case than in the isentropic (i.e. reversible) case.

To simplify notations, turbomachines will be considered having the same polytropic efficiency.

3.2. Loading

In order to illustrate the effect of turbomachine irreversibilities, the Figure 5 represents the Brayton thermodynamic cycle of the loading period with 90% polytropic efficiency, superposed with the ideal isentropic (i.e. reversible) Brayton cycle, which have 100% polytropic efficiency. Because irreversibilities in turbomachines increase their outlet temperature, T_1 is greater than T_{1is}, resulting in a greater ΔT_{comp}, meaning that a greater work is needed to achieve the same compression. Similarly, T_3 is greater than T_{3is}, resulting in a lower ΔT_{turb}, meaning the same expansion delivers a lower work.

With the previous notation, ΔT_{comp} and ΔT_{turb} writes:

$$\Delta T_{\text{comp}} = T_{2\text{nom}}\left(\psi^{1/\eta} - 1\right) \quad (4)$$

$$\Delta T_{\text{turb}} = T_{0\text{nom}}\left(\psi^{-\eta} - 1\right) \quad (5)$$

The specific energy stored during the loading then is:

$$e_{\text{load}} = c_{\text{p}}\left(\Delta T_{\text{comp}} + \Delta T_{\text{turb}}\right) = c_{\text{p}}\left(T_{2\text{nom}}\left(\psi^{1/\eta} - 1\right) + T_{0\text{nom}}\left(\psi^{-\eta} - 1\right)\right) \quad (6)$$

3.3. Delivery

The temperature T_2 and T_0 during the delivery writes:

$$T_2 = \psi^{-\eta} \times T_1 = \psi^{-\eta} \times \psi^{1/\eta} \times T_{2\text{nom}} \quad (7)$$

$$T_0 = \psi^{1/\eta} \times T_3 = \psi^{1/\eta} \times \psi^{-\eta} \times T_{0\text{nom}} \quad (8)$$

Because ψ is by definition greater than 1 and η is lower than 1, equations (7) and (8) implies that T_2 is greater than $T_{2\text{nom}}$ and T_0 is greater $T_{0\text{nom}}$. To avoid the cycle temperatures to be higher each cycles, it is necessary to bring T_2 back to $T_{2\text{nom}}$ and T_0 back to $T_{0\text{nom}}$, which should be done by the cold and the hot exchangers. However, given that it is not convenient to cool a gas at a high temperature, we would rather have T_2 equal to $T_{2\text{nom}}$, and do all the necessary cooling at the ambient temperature $T_{0\text{nom}}$.

According to equations (7) and (8), introducing a different thermal compression ratio during delivery period, noted ψ_{deliv}, allows to have T_2 equal to $T_{2\text{nom}}$. This implies:

$$\psi_{\text{deliv}} = \psi^{1/\eta^2} \quad (9)$$

Thus:

$$T_2 = T_{2\text{nom}} \quad (10)$$

$$T_0 = \psi_{\text{deliv}}^{1/\eta} \times \psi^{-\eta} \times T_{0\text{nom}} = \psi^{1/\eta^3 - \eta} \times T_{0\text{nom}} \quad (11)$$

Choosing a thermal compression ratio as defined in equation (9) allows the gap between T_2 and $T_{2\text{nom}}$ to reduce to zero, while the gap between T_0 and $T_{0\text{nom}}$ is increased. This allows all the irreversible heat to be evacuated at the ambient temperature $T_{0\text{nom}}$.

ΔT_{comp} and ΔT_{turb} then writes:

$$\Delta T_{\text{comp}} = T_0 - T_3 = T_{0\text{nom}}\left(\psi^{1/\eta^3 - \eta} - \psi^{-\eta}\right) \quad (12)$$

$$\Delta T_{\text{turb}} = T_1 - T_{2\text{nom}} = T_{2\text{nom}}\left(\psi^{1/\eta} - 1\right) \quad (13)$$

Finally, the delivered specific energy is:

$$e_{\text{deliv}} = c_{\text{p}}\left(\Delta T_{\text{comp}} + \Delta T_{\text{turb}}\right) = c_{\text{p}}\left(T_{0\text{nom}}\left(\psi^{1/\eta^3 - \eta} - \psi^{-\eta}\right) + T_{2\text{nom}}\left(1 - \psi^{1/\eta}\right)\right) \quad (14)$$

3.4. Storage efficiency

It is now straightforward to deduce the global storage efficiency, which is the ratio of the delivered specific energy, given in equation (14), to the loaded specific energy, given in equation (6). Actually, this theoretical efficiency results of the assumption that the same mass of gas is passed through the turbomachines during the two periods.

T_1 is the highest temperature of the process and thus will be limited by technical performances of the different components of the cycle, particularly the hot turbomachines. It is then convenient to write the theoretical efficiency ε_{th}, as a function of T_1 instead of T_{2nom}:

$$\varepsilon_{th}\left(T_{0nom}, T_1, \psi, \eta\right) = 1 + \frac{T_{0nom}\left(1-\psi^{(1/\eta^3)-\eta}\right)}{T_1\left(1-\psi^{-1/\eta}\right)+T_{0nom}\left(\psi^{-\eta}-1\right)} \tag{15}$$

Since this theoretical efficiency does not take the thermal front natural enlargement into account, the real efficiency ε will be lower than ε_{th}.

There are two approaches to reach a reasonable global storage efficiency of 70%, which is that reached by a pumped hydraulic storage system (PHS). T_1 may be low with a high η (for example, $\eta \approx 0.94$ and $T_1 \approx 320°C$), or T_1 may be high, with a low η (for example $\eta \approx 0.84$ and $T_1 \approx 1050°C$) (Figure 7). In other words, high temperatures can make up for low turbomachines polytropic efficiency.

4. Description of the model

The previous thermodynamic analysis does not describe transient phenomena, which play a critical role in the system behavior. Pressures should not stay constant during one cycle. Moreover, the thermal fronts tend to enlarge, due to convective heat exchanges and thermal diffusivity.

A one dimensional finite volume method has been employed for the discretization of the tanks.

4.1. Geometry

In Figure 8, the dead volumes symbolize the pipes linking the tanks and the turbomachines. Heat exchangers and turbomachines are not considered as volumes, as they are linking equations between dead volumes.

A simple geometry has been assumed to model the convective heat exchange in the tanks. It consists of a regular square array of square sub-channels (Figure 9).

In this geometry, the exchanged thermal power density is:

$$\mathcal{P}(z) = \frac{h \times \Delta S_{exch} \times \left(T_f(z) - T_s(z)\right)}{\Delta V} \tag{16}$$

With:

$$h = \frac{\mathrm{Nu} \times \lambda_\mathrm{f}}{d_\mathrm{h}} \tag{17}$$

$$\frac{\Delta S_\mathrm{exch}}{\Delta V} = \frac{4\Delta z\, d_\mathrm{h} N_\mathrm{ch}}{\Delta z \left(W_\mathrm{tank}\right)^2} = \frac{4 d_\mathrm{h} W_\mathrm{tank}{}^2 / L_\mathrm{ch}{}^2}{\left(W_\mathrm{tank}\right)^2} = 4\frac{d_\mathrm{h}}{L_\mathrm{ch}{}^2} \tag{18}$$

Thus:

$$\mathcal{P}(z) = 4\frac{\mathrm{Nu}\lambda_\mathrm{f}}{L_\mathrm{ch}{}^2}\left(T_\mathrm{f}(z) - T_\mathrm{s}(z)\right) \tag{19}$$

4.2. Hypothesis

The gas is assumed ideal, while compression and expansion are assumed to be adiabatic and irreversible. The system insulation is supposed ideal. We suppose that the only internal heat exchanges are the forced convection heat exchange between the gas and the solid, and thermal diffusion inside the solid walls. Gas and solid properties are assumed constant.

We also assume that the temperature of the solid is uniform in an elementary volume. This is equivalent to assume that the thermal resistance to the horizontal heat transfer is dominated by the surface resistance [13].

The relative influence of the surface and solid resistance to heat transfer is measured by the *Biot* number:

$$\mathrm{Bi} = \frac{h\delta}{\lambda_\mathrm{s}} \tag{20}$$

where δ is the half-thickness of the walls. Considering the geometry shown in Figure 9 :

$$\delta = \frac{L_\mathrm{ch} - d_\mathrm{h}}{2} \tag{21}$$

$$\alpha = \frac{\left(d_\mathrm{h}\right)^2}{\left(L_\mathrm{ch}\right)^2} \tag{22}$$

and with equation (17), Bi becomes:

$$\mathrm{Bi} = \frac{\mathrm{Nu}}{2}\frac{\lambda_\mathrm{f}}{\lambda_\mathrm{s}}\left(\alpha^{-1/2} - 1\right) \tag{23}$$

which is a monotonous decreasing function of α. Our problem is characterized by α greater than 0.1, thus the Biot number will remain smaller than its value when α = 0.1, which is 0.065. This ensures that temperature inside the wall is almost constant at a given altitude.

4.3. Equations and boundary conditions

The equations in the tanks are:

$$\frac{\partial(\rho_f)}{\partial t}+\frac{\partial(\rho_f v_f)}{\partial z}=0 \tag{24}$$

$$\frac{\partial(\rho_f T_f)}{\partial t}+\frac{\partial(\rho_f v_f T_f)}{\partial z}=\frac{4\mathrm{Nu}\lambda_f}{c_{p\_f}(d_h)^2}(T_s-T_f) \tag{25}$$

$$\frac{\partial(\rho_s c_{p\_s} T_s)}{\partial t}+\frac{\partial}{\partial z}\left(\lambda_s\frac{\partial T_s}{\partial z}\right)=\frac{\alpha}{1-\alpha}\frac{4\mathrm{Nu}\lambda_f}{(d_h)^2}(T_f-T_s) \tag{26}$$

$$\frac{\partial P}{\partial z}=-\frac{4f}{d_h}\frac{1}{2}\rho v^2 \tag{27}$$

$$P=\rho_f r T_f \tag{28}$$

where equation (24) is the mass conservation while (25) and (26) ensure energy conservation inside the gas and the solid. Regular hydraulic head losses are taken into account through equation (27) and equation (28) is the ideal gas law.

Since there is no refractory material in the dead volumes, equations are the same, but without equation (26) and with equation (25) becoming:

$$\frac{\partial(\rho_f T_f)}{\partial t}+\frac{\partial(\rho_f v_f T_f)}{\partial z}=0 \tag{29}$$

The boundary conditions are given by two characteristic equations of the two turbomachines (usually used to model such machines [14]), the two compression and expansion equations (2) and (3), and heat exchanger equations. So far, no convenient manufacturer data have been retrieved, so the characteristic equations are simulated with parabola for compressor, and exponentials and cubic spline interpolation for turbine, so that it reproduces the general aspect of typical turbomachine maps.

Turbomachine characteristics link the inlet and outlet pressures, and mass outputs:

$$\begin{cases} P_{outlet}=P_{inlet}\times f_{charac1}(\dot{m}_r) \\ \dot{m}_{inlet}=\dot{m}_{outlet}=\dot{m} \\ \eta=f_{charac2}(\dot{m}_r) \end{cases} \tag{30}$$

Exchangers are considered ideal, with no hydraulic head losses, and with outlet temperature equal to the set point temperature, so their equations are:

$$\begin{cases} \dot{m}_{outlet}=\dot{m}_{inlet} \\ P_{outlet}=P_{inlet} \\ T_{outlet}=T_{set\ point} \end{cases} \tag{31}$$

4.4. Numerical method

The model is based on a uniformly meshed one-dimensional finite volume approach (Figure 8), using an implicit centered scheme. Discretized equations are solved by the Newton-Raphson method. The model has been developed using MATLAB and compiled C code for computational intensive parts: computation of the Jacobian matrix, and sparse linear system resolution using KLU [15]. KLU is an effective matrix factorization algorithm for sparse matrices with very little fill-in, faster than default methods that use the Basic Linear Algebra Subprograms BLAS [16].

5. Results and discussions

This section presents the results obtained for an installation having a large storage capacity and power. Table 1 shows the main parameters of this problem.

Figure 10 shows the stored energy E_{network1} and the delivered energy E_{network2} of each of the successive cycles. The periodic steady state is reached after about ten cycles. The transient cycles last longer than the stabilized cycles, so these ten first cycles corresponds to 145 hours.

Figure 11 shows the evolution of the temperatures T_1, T_2, T_3 and T_4 during two stabilized cycles. T_2 and T_4 are the inlet temperatures of the heat exchangers. During loading, T_1 and T_3 are constant because their incoming gas has been regulated by the heat exchangers. That is not the case for T_2 and T_4, so when the thermal fronts approach the ends of the tanks, variations appear. During delivery, T_1 and T_3 are no longer regulated, and at the end of the delivery period, they show variations too, as do the inlet heat exchangers temperatures T_2 and T_4.

The time evolution of the high and low pressures is globally increasing during the loading and decreasing for the delivery period. This can be explained by the mean temperature of the system, which is higher in the loaded than in the “unloaded” system. Moreover, since the head losses are very small due to the small gas velocity in the channels, pressure is quasi-uniform in one tank.

The time evolution of the mass flow rate is similar to the evolution of pressures. This is due to the turbomachines mass flow rate, which are proportional to their inlet pressure:

$$\dot{m} = \dot{m}_{\text{r}}\, P_{\text{inlet}} \Big/ \sqrt{T_{\text{inlet}}} \tag{32}$$

Figure 12 presents the temperature profiles in the tanks, at the end of the loading and delivery period, in the steady periodic state. The computation of the temperature differences $\overline{\Delta T_{HP}}$ and $\overline{\Delta T_{LP}}$ allows writing the thermal energy stored/delivered by each tank, ΔE_{HP} and ΔE_{LP}:

$$\Delta E_{HP} = \rho_{\text{s}} \times (1-\alpha) \times H_{\text{tank}} \times (W_{\text{tank}})^2 \times c_{\text{p\_s}} \times \overline{\Delta T_{HP}} \tag{33}$$

$$\Delta E_{LP} = \rho_{\text{s}} \times (1-\alpha) \times H_{\text{tank}} \times (W_{\text{tank}})^2 \times c_{\text{p\_s}} \times \overline{\Delta T_{LP}} \tag{34}$$

The system total energy difference between the end of the loading and the end of the delivery period is then:

$$\Delta E_{\text{tot}} = \Delta E_{\text{HP}} - \Delta E_{\text{LP}} \tag{35}$$

During the delivery period, the restored energy E_{network2} is $\Delta E_{\text{tot,}}$ minus the thermal losses in the cold exchanger, E_{cool2}:

$$E_{\text{network2}} = \Delta E_{\text{tot}} - E_{\text{cool2}} \tag{36}$$

Then, the global storage efficiency writes:

$$\varepsilon = 1 - \frac{E_{\text{cool1}} + E_{\text{cool2}}}{\Delta E_{\text{tot}} + E_{\text{cool1}}} \tag{37}$$

Figure 12 b) shows that the gap allowed by the relative threshold *Tol* has been exceeded at the bottom of the tank, triggering the end of the loading period. This temperature difference is representative of the thermal losses E_{cool1} (Figure 4). In Figure 12 a), the allowed gap is also exceeded at the bottom of the tank, triggering the end of the delivery period. This temperature difference is representative of a part of the thermal losses E_{cool2}. At the top of the tanks, the temperatures stayed in the allowed gaps and didn't trigger anything.

According to equation (37), in order to improve the efficiency and get closer to the theoretical efficiency given in equation (15), ΔE_{tot} must be increased whereas E_{cool1} and E_{cool2} are decreased or kept constant. This implies increasing ΔE_{HP} and ΔE_{LP}, thus increasing the thermal front gradient dT/dz, which finally means increasing the exchanged thermal power density in the channels. According to equation (19), this can be done in two ways: decreasing the channel longitudinal dimension L_{ch}, or increasing the Nusselt number.

Since the tanks internal geometry, the flow state (turbulent or laminar), and the refractories physical properties all have to be optimized, the results presented here should be improved in the future. Particularly, turbulence generation in the channels could increase the Nusselt number, and the use of a packed bed regenerator could decrease the hydraulic diameter. Those two modifications will also increase the hydraulic head losses, but with a possibly negligible impact since they are currently very small.
Moreover, the thermal conductivity of argon is currently assumed independent of temperature. Actually, it is about three times larger at 1000°C than at 20°C, what would also increase the exchanged thermal power density and improve the process performance significantly. Taking into account the temperature dependencies in the developed model is straightforward and new results will be available soon.

6. Conclusion

A new type of thermal energy storage process for large scale electric applications has been presented. The storage principle has been exposed, and the expression of the theoretical storage efficiency was given based on an analysis of the involved thermodynamic cycles. A numerical model has been developed, showing the feasibility of the process, even with sub-optimal parameters, basic geometry, and laminar convective heat transfer. Moreover, the

development of reciprocating compressors and turbines with higher polytropic efficiencies could lead to lower temperature and smaller scale applications still showing decent efficiencies. Finally, the increase of the heat exchange is identified as a key factor to approach the theoretical storage efficiency, through the increase of the Nusselt number and the heat transfer area. Solutions such as turbulence generation or the use of packed bed regenerators are to be investigated. The validation of the model requires a test loop including two sufficiently large regenerators. Such a test loop already exists at CEA Grenoble, and will be available in a close future.

Our results allow to compare our large scale process with the two mature other ones, namely PHS and CAES. PHS offers great electric capacity, power, and efficiency, with relatively low investment, considering an already built dam, having two sufficiently large upstream and downstream water reservoirs available. CAES also presents large scale electric capacity and power, but it is not really comparable, since natural gas is used to heat compressed air during the delivery period. This issue is resolved in the research project Advanced Adiabatic Compressed Air Energy Storage (AA-CAES) [17], where the compression heat is stored in a TES unit, and released to preheat compressed air during the delivery period.

However, suitable PHS sites are not very frequent and generally already exploited, at least in occidental countries. Moreover, exploiting new sites often leads to environmental issues. About CAES, there also are requirements for site choice, such as the presence of a large cavity with convenient geological properties.

Our process suffers for practically no geographical or geological constraints and no safety or environmental issues, and seems to be able to reach similar efficiency, capacity and power performances.

References

[1] H. Chen, T.N. Cong, W. Yang, C. Tan, Y. Li, and Y. Ding, “Progress in electrical energy storage system: A critical review,” Progress in Natural Science, vol. 19, March 2009, pp. 291-312.

[2] H. Ibrahim, A. Ilinca, and J. Perron, “Energy storage systems--Characteristics and comparisons,” Renewable and Sustainable Energy Reviews, vol. 12, June 2008, pp. 1221-1250.

[3] V.V. Tyagi and D. Buddhi, “PCM thermal storage in buildings: A state of art,” Renewable and Sustainable Energy Reviews, vol. 11, August 2007, pp. 1146-1166.

[4] D.S. Sowmy and R.T. Prado, “Assessment of energy efficiency in electric storage water heaters,” Energy and Buildings, vol. 40, 2008, pp. 2128-2132.

[5] Y. Reboussin, J.F. Fourmigué, P. Marty, and O. Citti, “A numerical approach for the study of glass furnace regenerators,” Applied Thermal Engineering, vol. 25, October 2005, pp. 2299-2320.

[6] H. El Qarnia, “Numerical analysis of a coupled solar collector latent heat storage unit using various phase change materials for heating the water,” Energy Conversion and Management, vol. 50, February 2009, pp. 247-254.

[7] A.F. Regin, S. Solanki, and J. Saini, “Latent heat thermal energy storage using cylindrical capsule: Numerical and experimental investigations,” Renewable Energy, vol. 31, October 2006, pp. 2025-2041.

[8] R. Kandasamy, X. Wang, and A.S. Mujumdar, “Transient cooling of electronics using phase change material (PCM)-based heat sinks,” Applied Thermal Engineering, vol. 28, June 2008, pp. 1047-1057.

[9] P. Denholm and T. Holloway, “Improved Accounting of Emissions from Utility Energy Storage System Operation,” Environmental Science & Technology, vol. 39, December 2005, pp. 9016-9022.

[10] P. Denholm and G.L. Kulcinski, “Life cycle energy requirements and greenhouse gas emissions from large scale energy storage systems,” Energy Conversion and Management, vol. 45, August 2004, pp. 2153-2172.

[11] W. Ma, Y. Liu, M. Su, and N. Yu, “Multi-stage axial flow compressors characteristics estimation based on system identification,” Energy Conversion and Management, vol. 49, February 2008, pp. 143-150.
[12] René Bidard and Jacques Bonnin, Energétique et turbomachines, EYROLLES, 1979.
[13] A. John Willmott, Dynamics of Regenerative Heat Transfer, Taylor & Francis, 2001.
[14] Renaud Gicquel, Systèmes énergétiques, Les presses de l'Ecole des Mines, 2001.
[15] Tim Davis, “Sparse LU factorization of circuit simulation matrices,” http://www.cise.ufl.edu/~davis/techreports/KLU/pp04.pdf, Feb. 2004.
[16] Iain S. Duff, Michael A. Heroux, and Roldan Pozo, “An overview of the Sparse Basic Linear Algebra Subprograms: The new standard from the BLAS Technical Forum,” ACM TRANS. MATH. SOFTW, vol. 28, June 2002, pp. 239--267.
[17] Chris Bullough, Christoph Gatzen, Christoph Jakiel, Martin Koller, Andreas Nowi, and Stefan Zunft, “Advanced Adiabatic Compressed Air Energy Storage for the Integration of Wind Energy,” Proceedings of the European Wind Energy Conference, London UK.: 2004

Capacity	$E_{network2}$ = 602.6 MWh
Storage efficiency	ε = 66.7%
Theoretical Storage efficiency	ε_{th} = 81.6%
Loading duration	6h03
Delivery duration	5h52
Tanks volume	21 622 m^3
Turbomachines Polytropic efficiency	η = 0.9
Tanks void fraction	α = 0.44
Maximum Pressure reached	P_{max} = 4.6 bars
Maximum Temperature reached	T_{max} = 1268 K

Table 1: Main parameters of the problem

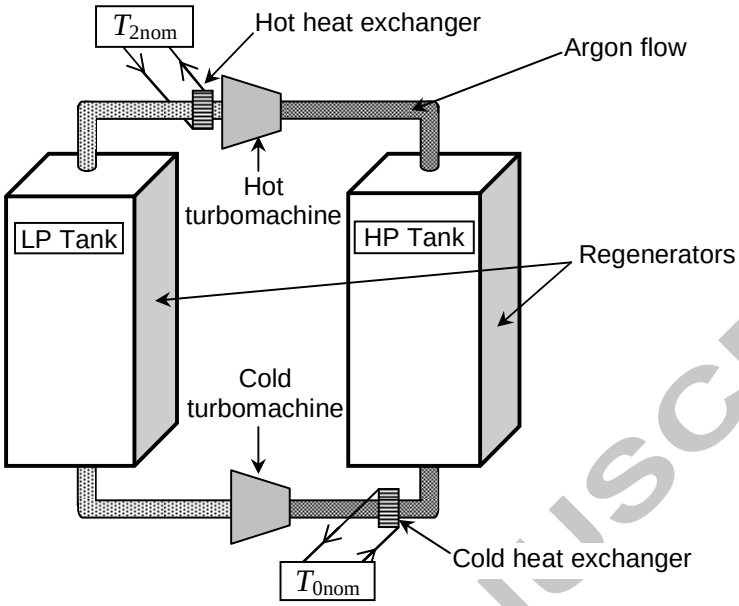

Figure 1 : Schematic representation of the storage principle.

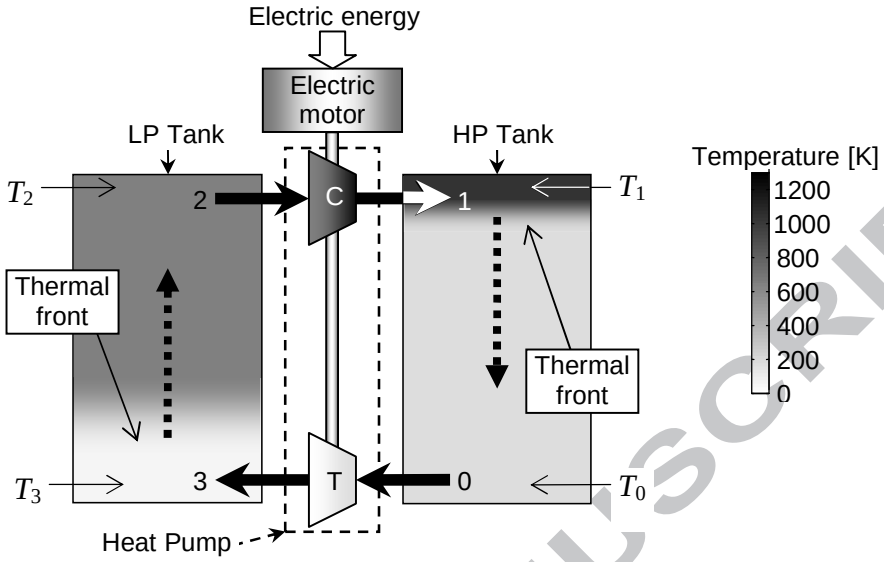

Figure 2: During the loading period, the gas flow clockwise, following an energy-consuming Brayton heat pump cycle.

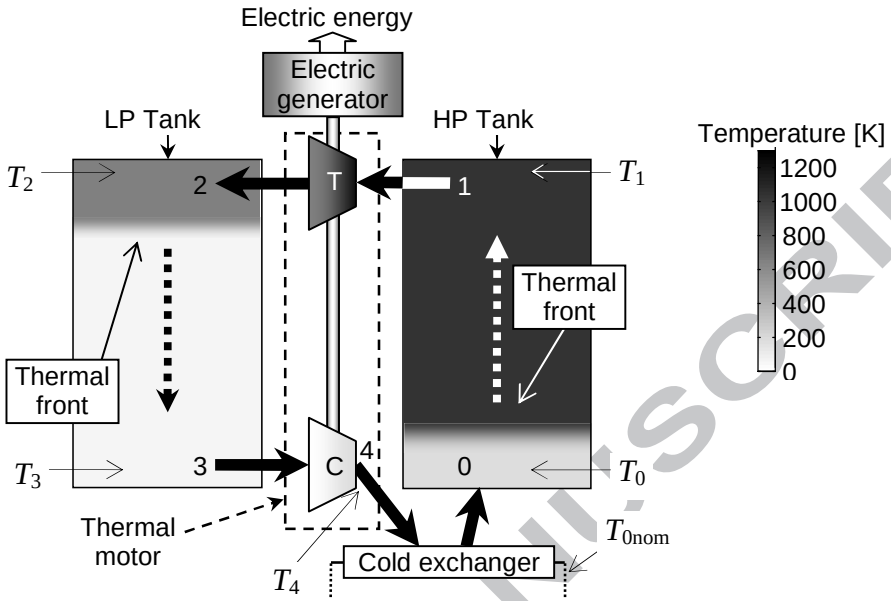

Figure 3: During the delivery period, the gas flows counter-clockwise, following an energy-generating Brayton heat engine cycle.

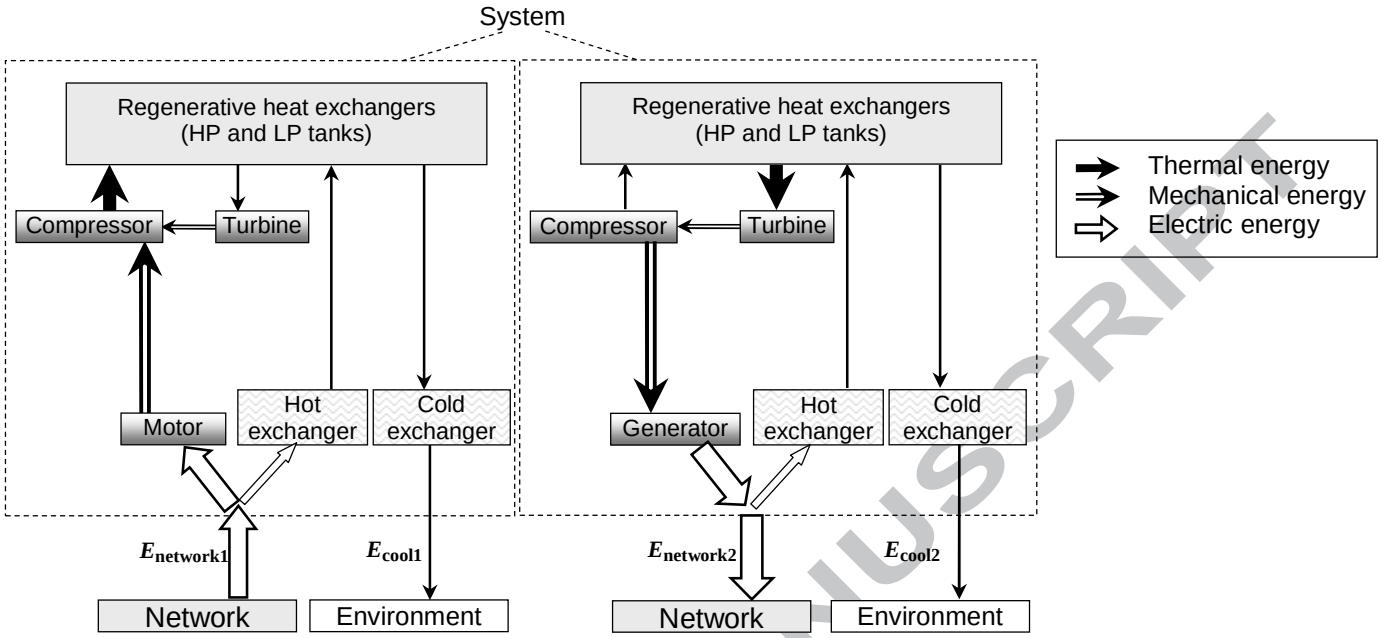

a) Loading **b) Delivery**

Figure 4 : Flow chart of the exchanges of energy

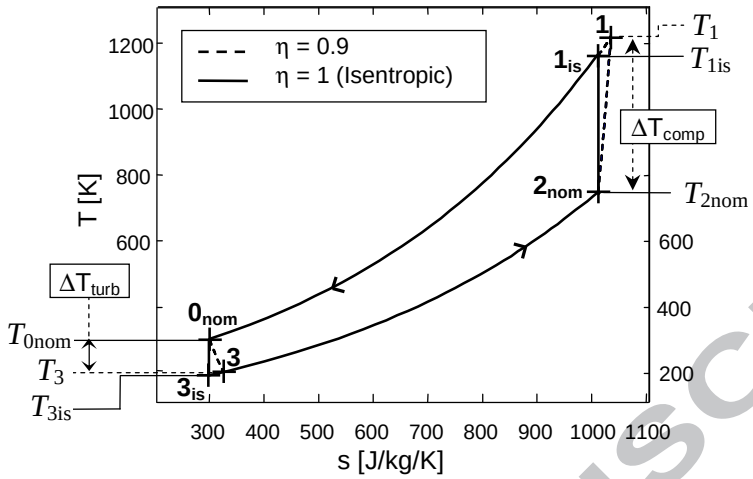

Figure 5: Superposition of reversible and irreversible heat pump Brayton cycle. Specific entropy reference is arbitrary.

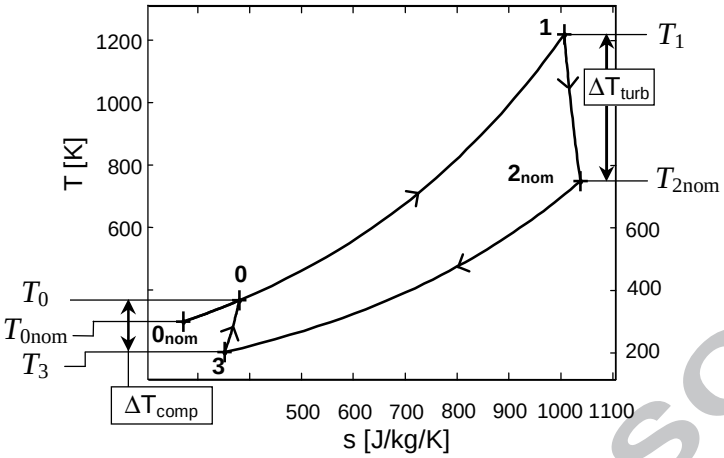

Figure 6: Thermodynamic diagram of the delivery period.

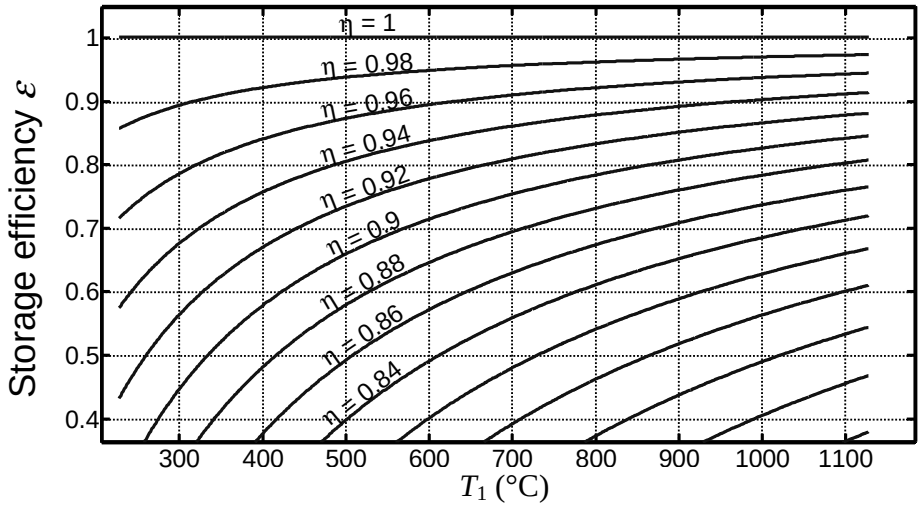

Figure 7: storage efficiency as a function of T_1 and η, with $T_{2\mathrm{nom}} = 20°\mathrm{C}$, $\psi = 1.55$

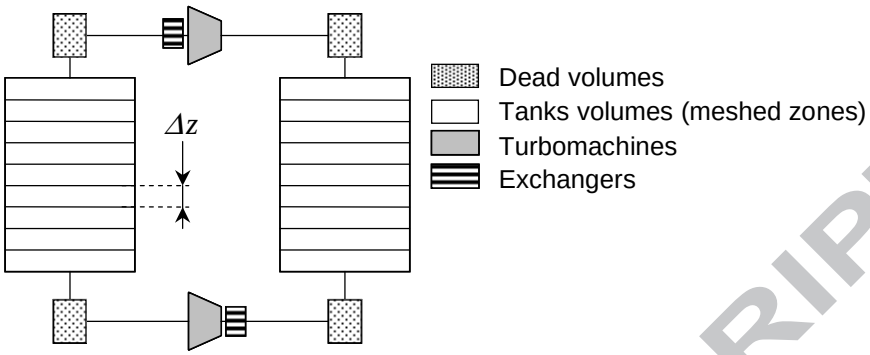

Figure 8: Geometry and links between finite volumes

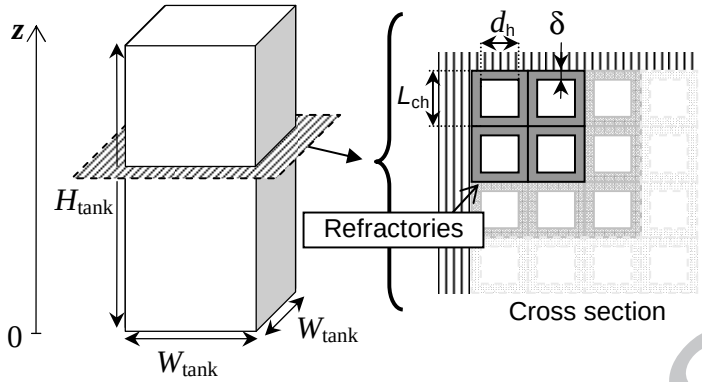

Figure 9: Cross sectional view of the tanks, showing the square sub-channels network.

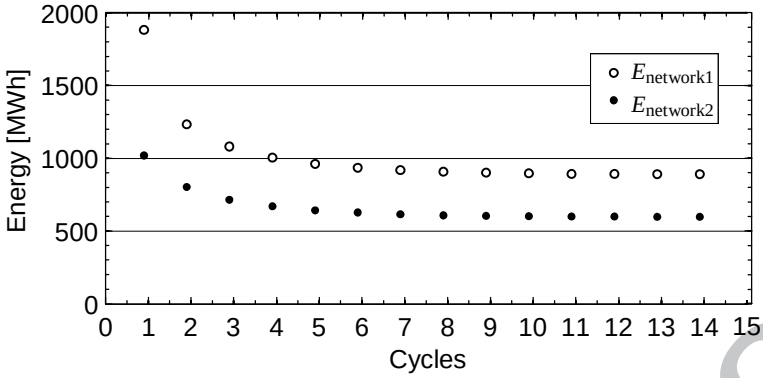

Figure 10 : Evolution of the stored and restored energy with cycles

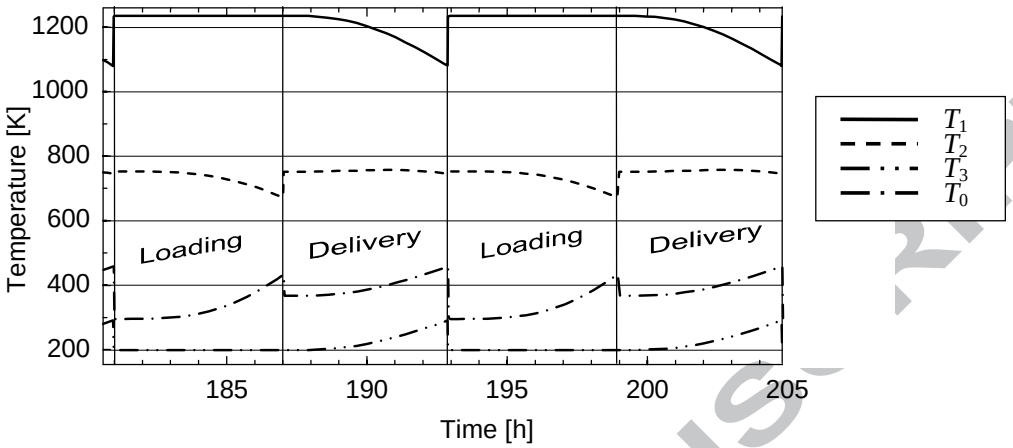

Figure 11 : Evolution of T_1, T_2, T_3 and T_4 during two stabilized cycles.

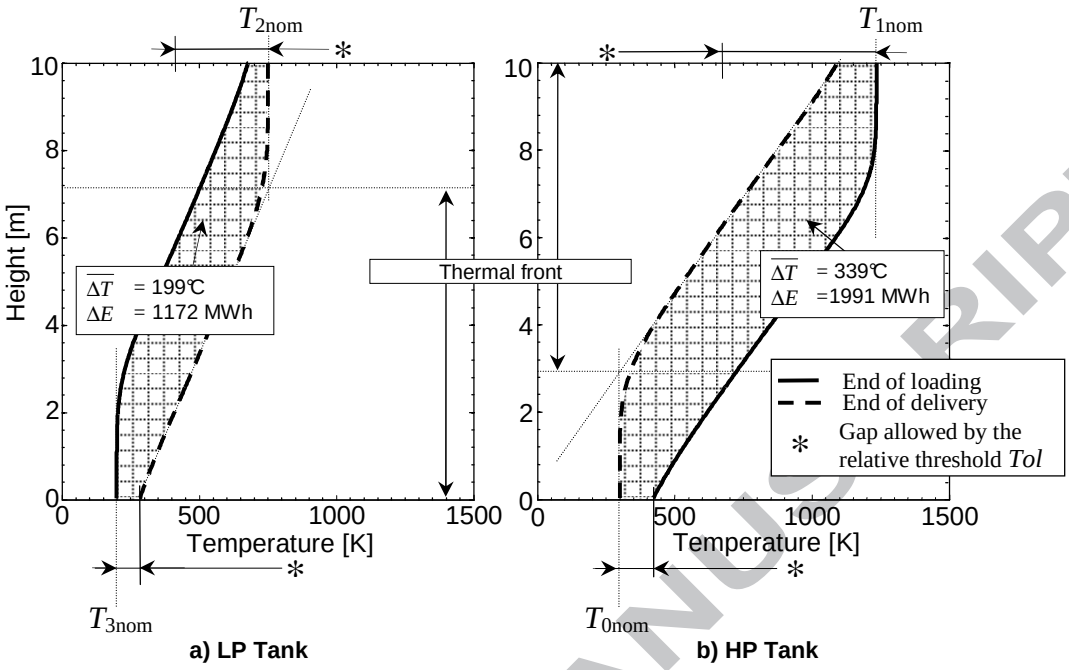

Figure 12 : Temperature profile at the end of the loading and delivery period.